Experimental and optimization investigations of multi cycle interrupted borocarburizing process

G. Surya Raj

Assistant Professor, Department of Mechanical Engineering, Park College of Engineering and Technology, Anna University, 641659 Tamil Nadu, India.

M. Prince

Principal and Professor, Department of Mechanical Engineering, Tamilnadu College of Engineering, Anna University, 641659 Tamil Nadu, India.

Received 24 January 2026; accepted 13 April 2026

Multi-cycle interrupted borocarburizing, a modified pack boriding technique, enhances AISI 1015 steel by improving strength while maintaining surface microhardness. Using response surface methodology, the effects of temperature, time, and cycles on microhardness and tensile strength were optimized. A regression model based on central composite design showed strong experimental agreement. MCIBC layers exhibited distinct iron boride and carburized zones, with microhardness values of $1410\,\mathrm{HV}_{0.05}$ in the iron boride zone, $650\,\mathrm{HV}_{0.05}$ in the carburized zone, and $210\,\mathrm{HV}_{0.05}$ in the base metal. Unlike continuous boriding, MCIBC layers showed no needle-like structure and had a gradual hardness gradient. XRD analysis revealed Fe_3C, Fe_2B, and FeB phases. MCIBC achieved a 1.23 times improvement in tensile strength (488 MPa vs. 395.8 MPa). This study demonstrates MCIBC superiority in balancing ultimate tensile strength and microhardness compared to continuous pack boriding.

Keywords: Boriding; microhardness; microstructure; borocarburizing; strength.

DOI: https://doi.org/10.31349/RevMexFis.72.041007

1. Introduction

Pack boriding is one of the popular thermochemical surface modification treatments for enhancing the surface hardness of the steel and its alloys (Kusmanov et al., 2016). In general, pack boriding process offer extremely higher hardness on the surface of the steel as compared with the conventional, plasma-based carburizing and nitriding processes (Nora *et al*., 2019). The pack boriding process is carried out at a temperature in the range of 780°C to 1100°C for 1 h to 10 h depending upon the case depth and hardness requirements (Rai *et al*., 2017). During the pack boriding process, boron atoms are diffused into the surface of the steel and forms a hard boride layer (Prince *et al*., 2022). Due to boron diffusion into the steel, the surface is enriched with boron atoms (Jurci *et al*., 2020). The iron borides such as Fe_2B (8.3% B) and FeB (16.7%) are formed on the surface of the steel based on the boron enrichment as a result of boron diffusion (Hernandaz Sanchez *et al*., 2014). The iron borides exhibit low coefficient of friction combined with excellent wear, corrosion and oxidation resistance (Garcia-Leon *et al*., 2021; Rayane *et al*., 2017). The researchers have reported that the pack boriding process reduces the ductility, strength and toughness of the steels due to brittleness (Prince *et al*., 2019). The researchers have reviewed the reasons for brittleness generated in the steel during pack boriding process. Also, they have attempted to solve this problem using various methodologies such as Ion beam (Winter *et al*., 2015), electron beam (Santana *et al*., 2020), Diffusion annealing (Campos-silva *et al*., 2017), laser boriding (Prince *et al* 2018; Kulka *et al*., 2015), Interrupted Boriding (Gopalakrishnan *et al*., 2002; Calik *et al*., 2017) and various multicomponent treatments (Sizov *et al*., 2016). We have reviewed those methodologies to identify the research gap.

Despite, some of the material handling equipment (drill bits) and the machinery parts (gears, crankshafts, train wheels etc.) are highly demanded to meet the need of high hardness as well as high strength (Gunen *et al*., 2017; Vanegas *et al*., 2021). Accordingly, many researchers have highly been focused on the enhancement of Mechanical properties (Mathew *et al*., 2014; Kheyrodin *et al*., 2017) and improvement of Tribo properties (Erdogan *et al*., 2019; Krelling *et al*., 2017). However, many researchers were investigated the effect of multicomponent of boride layer, but they are failed to study the effect of cooling behavior and the effect of carbon in the precarburized steel simultaneously.

Researchers have attempted many methods to reduce brittleness in order to improve the ductility, strength and toughness of borided AISI 1015 steel However, those methods enhance either ductility or strength or toughness or combination of properties by compromising the surface hardness. To address this research gap, a novel treatment called Multi Cycle Interrupted Borocarburizing Process (MCIBC) has been developed. However, no one can optimize the multiple parameters of Hardness and Tensile Strength simultaneously on interrupted borocarburized steels and minimal studies have been conducted about tensile strength (Khari *et al*., 2017; Montgomery 2019).

The prospective line for forthcoming development of this process is to reduce the property of brittleness without much compromising the value of Hardness with an improvement of strength in the boride layer. This study analyzed the results of the Multi-Cycle Interrupted Borocarburizing Process (MCIBC) and Continuous Boriding (CB) to reduce brittleness and improve tensile strength in the boride layer. Structural properties such as microstructural morphology, XRD investigations, and mechanical properties such as Tensile test with Fractographic analysis, and Microhardness were analyzed.

2. Materials and methods

2.1. Base material

This work used commercially available carbon steel as the base material. The chemical composition was measured using a spectrometer. The cylindrical steel specimens were machined for a dimension of 25 mm in diameter and 12.5 mm in height. The specimens were metallographically well prepared as per the standard. The composition is given in Table I.

2.2. Process of multi cycle interrupted borocarburizing

First, the steel specimens were gas carburized at 930°C for 2 hours. The mixtures of methanol with acetone were used as a controlled medium for this process. The gas mixtures of methanol + acetone had fed at a flow rate of 50 l/h. The carbon potential was 0.65%. Next, the carburized specimens were interrupted borided using multicycle powder pack boriding method. The pack composition was 5wt.% B_4C, 5wt.%KBF_4, and 90wt.%SiC. The schematic of multicycle interrupted boriding process and experimental setup used in this investigation are shown in Figs. 1a) and 1b). The pre-carburized steel specimens were enclosed in a stainless-steel box and placed inside a graphite crucible containing silica sand. The crucible was loaded in a muffle furnace and the process time, temperature and number of cycles were chosen. The process time was varied from 60 min to 180 min, the temperature range was 850°C to 1050°C, and the number cycle was 1 to 3.

TABLE I. Chemical composition of the material (wt.%).

C	Si	Mn	P	S	Fe
0.152	0.246	0.689	0.017	0.001	Balanced

TABLE II. Criteria for MCIBC process using RSM technique

Factor	Unit	Level		
		-1	0	$+1$
Time (A)	Minutes	60	120	180
Temperature (B)	Celsius	850	950	1050
Number of cycle (C)	No unit	1	2	3

2.3. Response surface methodology

A response surface methodology (RSM) with a central composite design (CCD) was employed to optimize the three independent factors: time (A, 60-180 min), temperature (B, 850-1050°C), and number of cycles (C, 1-3). The design consisted of 20 experimental runs, including 8 factorial points (2^8), 6 axial points (star points), and 6 replicates at the center point. The axial distance (α) was set to 1.6817, making the design rotatable. The experimental matrix and the resulting responses for microhardness and ultimate tensile strength (UTS) are presented in Table III. A second-order quadratic polynomial model was fitted to the data.

The objective of this technique is to optimize the response (output variables) with respect to different independent variable (input variable) (Turkoglu *et al*., 2019), (Babu *et al*., 2015). When all independant variables are assumed to be measured with negligible error, the corresponding response should be stated in Eq. (1)

$$y = f(x_1, x_2, x_3, \ldots, x_i), \tag{1}$$

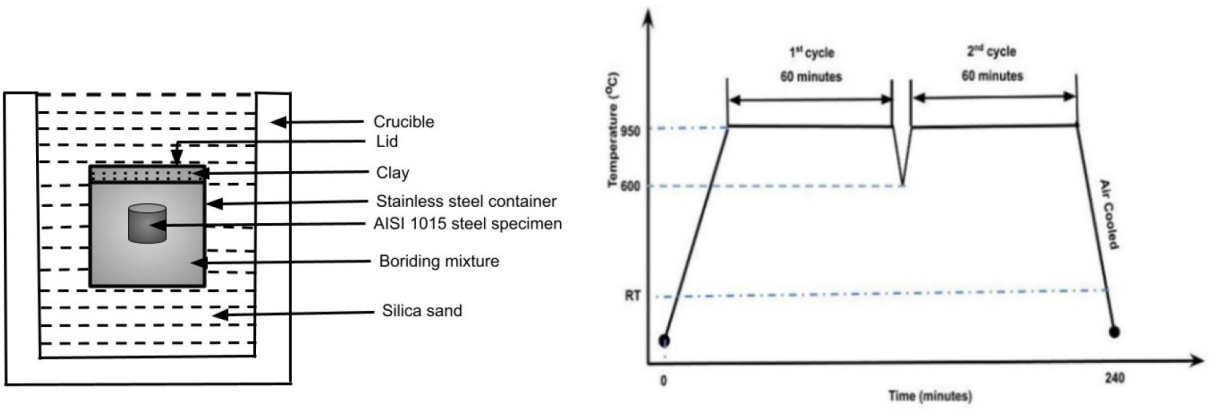

FIGURE 1. Schematic representation of a) the pack boriding experimental setup and b) the temperature–time cycle employed during the boriding process.

TABLE III. Experimental design matrix and measured responses

Std	Run	Factors			Responses	
		A: Time (min)	B: Temperature (°C)	C: No. of cycle (no unit)	Hardness (HV)	UTS (N/mm^2)
17	1	120	950	2	1469.52	451
8	2	180	1050	3	1662	436
10	3	220	950	2	1625	455
1	4	60	850	1	1285	457
9	5	30	950	2	1354	476
4	6	180	1050	1	1620	485
7	7	60	1050	3	1520	410.705
20	8	120	950	2	1465.52	454
18	9	120	950	2	1462.52	450
15	10	120	950	2	1473.52	458
2	11	180	850	1	1408	424.17
6	12	180	850	3	1532.5	436
16	13	120	950	2	1472.52	448
11	14	120	780	2	1250	363
12	15	120	1120	2	1590	432
19	16	120	950	2	1473.52	450
5	17	60	850	3	1338.72	425.465
13	18	120	950	1	1450	488.924
14	19	120	950	4	1507.92	438
3	20	60	1050	1	1426	514

where y is the response and x_i is the number of independent parameters which is known to be factor. In the actual application of RSM, an approximation model is built to maximize the response y. The approximating model is an empirical model that is based on data that has been seen in the system or process. A group of statistical methods known as multiple regression analysis can be used to create the empirical models needed by RSM. The second order polynomial equation are stated as

$$y = \beta_0 + \sum_{i=1}^{k} \beta_i x_i + \sum_{i<j}^{k} \beta_{ij} x_i x_j + \sum_{i=1}^{k} \beta_{ii} x_i^2 + \varepsilon, \quad (2)$$

where $\beta ij = 0, 1, 2, 3...$, k is known to be regression coefficients.The regression model which represents the link between input and output Parameter. The significance of the developed model had evaluated by analysis of Variance (ANOVA) technique (Atul *et al*., 2016). In this process, three level three factorial designs had carried out using design expert software (version 11.5). For each factor three design parameters are considered. The criteria for this process are mentioned in Table II. The optimum parameter value of this parameter had obtained based on the developed regression model. Following to which a numerical optimization had possessed for optimum parameter.

A response surface methodology (RSM) with a central composite design (CCD) was employed to optimize the three independent factors: time (A, 60-180 min), temperature (B, 850-1050°C), and number of cycles (C, 1-3). The design consisted of 20 experimental runs, including 8 factorial points (2), 6 axial points (star points), and 6 replicates at the center point. The axial distance (α) was set to 1.6817, making the design rotatable. The experimental matrix and the resulting responses for microhardness and ultimate tensile strength (UTS) are presented in Table III. A second-order quadratic polynomial model was fitted to the data.

2.4. Microstructural examination

The processed specimens were sliced perpendicularly to the treated surface and mounded for metallographic investigations. The surfaces of the samples were finely polished using 1200 grid of emery paper and etched using 3% Nital. The Microstructures of Continuous Boriding and MCIBC samples were captured using Dwinter optical microscope and metallographically polished samples as well as the behavior of the fractured surface in the tensile test were investigated using Carl Zeiss (USA) Scanning electron microscope.

2.5. Microhardness studies

Microhardness measurements were taken from surface to core using Vicker's Mitutoyo microhardness tester as per

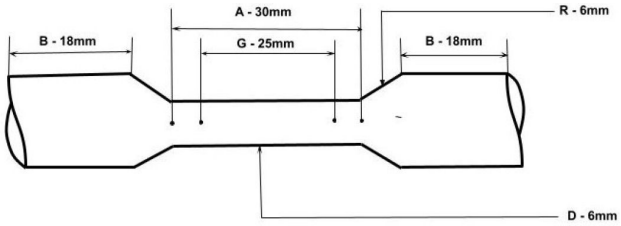

FIGURE 2. Schema of tensile sample.

ASTM E384 standard. 50 g load was used to study the hardness variation along the depth for continuous borided and MCIBC specimens. The graph was plotted against distance from the surface and microhardness.

2.6. XRD examination

The phase formation of continuous borided, and MCIBC processes was investigated by X-ray diffraction using CuKα with $\lambda = 1.54060$Å radiation.

2.7. Tensile test

The MCIBC and Continuous Boriding tensile specimens were tested using FIE universal tensile machine as per ASTM E8 standard. The minimum load and strain rate of 2KN and 10 mm/min were maintained respectively. The tensile parameters of both processes were studied and compared using SEM. The schematic diagram of standard tensile sample is shown in Fig. 2.

3. Results and discussions

3.1. Optimization of process parameters

The output responses such as Micro Hardness, and UTS had observed in Table III for MCIBC samples for different input parameters (Temperature, Time and Number of cycles). As per the matrix of three factor three level central composite design (Arguelles-ojeda *et al*., 2017), twenty experiments had processed out.

3.1.1. ANOVA for Vickers Hardness and Ultimate tensile strength

The purpose of ANOVA is to assess the models significance and to direct the design space (Turkoglu *et al*., 2019). Table IV and V provide the ANOVA details for Microhardness and Ultimate Tensile Strength. The associated models were considered significant, if the P value (significant probability value) was less than 0.5 and the F value was larger than 1(Sashank *et al*., 2019). Microhardness and Ultimate Tensile Strength of the MCIBC process have P values of 0.5 (95% confidence level), confirming that the entire model is statistically significant (Babu *et al*., 2015). The model's F values are 156.72 for microhardness and 54.13 for UTS. It displays all models with F values larger than one and confirms that they are significant. The measured R^2 value is about 1. As a result, the model is thought to be desirable (Sashank *et al*., 2019). The value of Microhardness (95.63%) 0.9563 and UTS (97.99%) 0.9799 R^2 showed higher agreement with the observed response within the experimental range. In which predicted R^2 values of microhardness and ultimate tensile strength (0.9181) and (0.8514) exhibited good agreement with adjusted R^2 values of microhardness and ultimate tensile strength (0.9481) and (0.9618), with a difference of less than 0.2 (Alam *et al*., 2020). As a result, the model is desired and statistically significant. The role of adequate Precision is to calculate the signal-to-noise ratio. A ratio larger than 4 was considered as optimal (Khuri *et al*., 2017). Microhardness precision is 37.0045 and UTS precision is 33.7374. It finds that the signal-to-noise ratio is greater than 4 on both parameters. As a result, the relevant values are statistically significant and appropriately traversed the design space.

The value of Coefficient of variance of microhardness and UTS are 1.69% and 1.37% respectively. The low proportion

TABLE IV. ANOVA for vickers microhardness.

Source	Sum of Squares	dof	Mean Square	F-value	p-value	Remark
Model	1.976×10^5	3	65866.10	156.72	< 0.0001	Significant
A: Time	82761.27	1	82761.27	196.93	< 0.0001	
B: Temperature	1.034×10^5	1	1.034×10^5	245.96	< 0.0001	
C: No. of cycle	11506.33	1	11506.33	27.38	< 0.0001	
Residual	6724.25	16	420.27			
Lack of Fit	5933.42	11	539.40	3.41	0.0932	Not significant
Pure Error	790.83	5	158.17			
Cor Total	2.043×10^5	19				
Std. Dev = 24.80		Mean = 1469.31		R^2 = 0.9563		
C.V. (%) = 1.69		Adj. R^2 = 0.9481		Pred. R^2 = 0.9189		
Adeq. Precision = 37.0045						

TABLE V. ANOVA for ultimate tensile strength.

Source	Sum of Squares	dof	Mean Square	F-value	p-value	Remark
Model	18421.26	9	2046.81	54.13	< 0.0001	Significant
A-Time	312.45	1	312.45	8.26	0.0165	
B-Temperature	3524.16	1	3524.16	93.20	< 0.0001	
C-No. of Cycle	5452.34	1	5452.34	144.19	< 0.0001	
AB	43.20	1	43.20	1.14	0.3103	
AC	1192.18	1	1192.18	31.53	0.0002	
BC	2197.51	1	2197.51	58.12	< 0.0001	
A^2	372.73	1	372.73	9.86	0.0105	
B^2	5288.68	1	5288.68	139.86	< 0.0001	
C^2	948.74	1	948.74	25.09	0.0005	
Residual	378.13	10	37.81			
Lack of Fit	313.30	5	62.66	4.83	0.0544	Not significant
Pure Error	64.83	5	12.97			
Cor Total	18799.39	19				
Std. Dev.	6.15	R-Squared	0.9799			
Mean	447.61	Adj. R-Square	0.9618			
C.V.%	1.37	Pred. R-Square	0.8514			
		Adeq. Precision	33.7473			

of COV indicates that the relevant model is more reliable and predictable than experimental values. Lack of Fit values for Microhardness are 3.41 and UTS is 4.83, respectively. Because the LOF values of the associated models are more than 0.05, their values are considered insignificant (Alam *et al*., 2020). The fundamental result of ANOVA for microhardness indicates Time (A), Temperature (B), and Number of Cycles (C) as significant models, and it meets the P Value less than 0.05 requirement. As a result, the microhardness model agrees rather well with the independent models and input response. Similarly, the ANOVA result for UTS represents Time (A), Temperature (B), and Number of Cycle (C), and the quadratic effect of Time (A^2), Temperature (B^2), and Number of Cycle (C^2), as well as interaction effect such as AC and BC are the influencing parameters of UTS. The P value of the corresponding models is less than 0.05. Although, the interaction effect of the Time (A) along with Temperature (B) exhibits some influence on the UTS, it might be considered as statistically insignificant model. As a result, the UTS model demonstrated reasonable agreement with the independent models and input response.

A regression equation was built for the associated parameters (microhardness and UTS) of the MCIBC Process, with the mathematical expression and variables A,B, and C.

The regression model of Microhardness (Actual Equation) and UTS are represented in Eqs. (3) and (4)

$$\begin{aligned}\text{Microhardness} &= 380.73711 + 1.38884\,A \\ &\quad + 0.901147\,B + 31.77154\,C, \qquad (3)\\ \text{UTS} &= -1501.17416 - 1.22697\,A + 4.00544\,B \\ &\quad + 76.58525\,C + 0.000387\,AB \\ &\quad + 0.203458\,AC - 0.165737\,BC \\ &\quad + 0.001542\,A^2 - 0.001874\,B^2 \\ &\quad + 8.41203\,C^2. \qquad (4)\end{aligned}$$

The regression model of Microhardness (Coded Equation) and UTS are represented in Eqs. (5) and (6)

$$\begin{aligned}\text{MicroHardness} &= 1467.03 + 83.33\,A + 90.11\,B \qquad (5)\\ &\quad + 31.77\,C, \qquad (6)\\ \text{UTS} &= 452.62 - 4.92\,A + 15.99\,B - 22.80\,C \\ &\quad + 2.32\,AB + 12.21\,AC - 16.57\,BC \\ &\quad + 5.55\,A^2 - 18.74\,B^2 + 8.41\,C^2. \qquad (7)\end{aligned}$$

The interaction effect is displayed using a 2D contour plot and a 3D surface plot, and the output response of the microhardness and UTS of MCIBC samples is shown in Figs. 3 and 4. There were four distinct numbers of cycles handled in

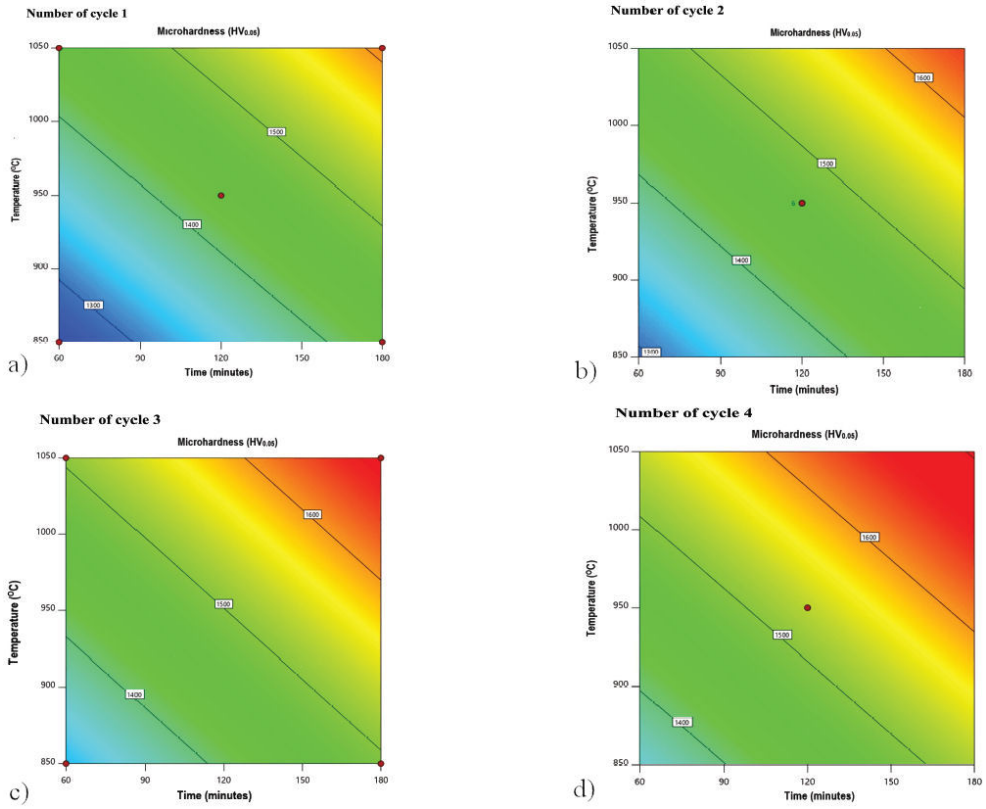

FIGURE 3. Response surface plots showing the combined effect of temperature and time on microhardness ($HV_{0.05}$) for different numbers of cycles: a) cycle 1, b) cycle 2, c) cycle 3, and d) cycle 4.

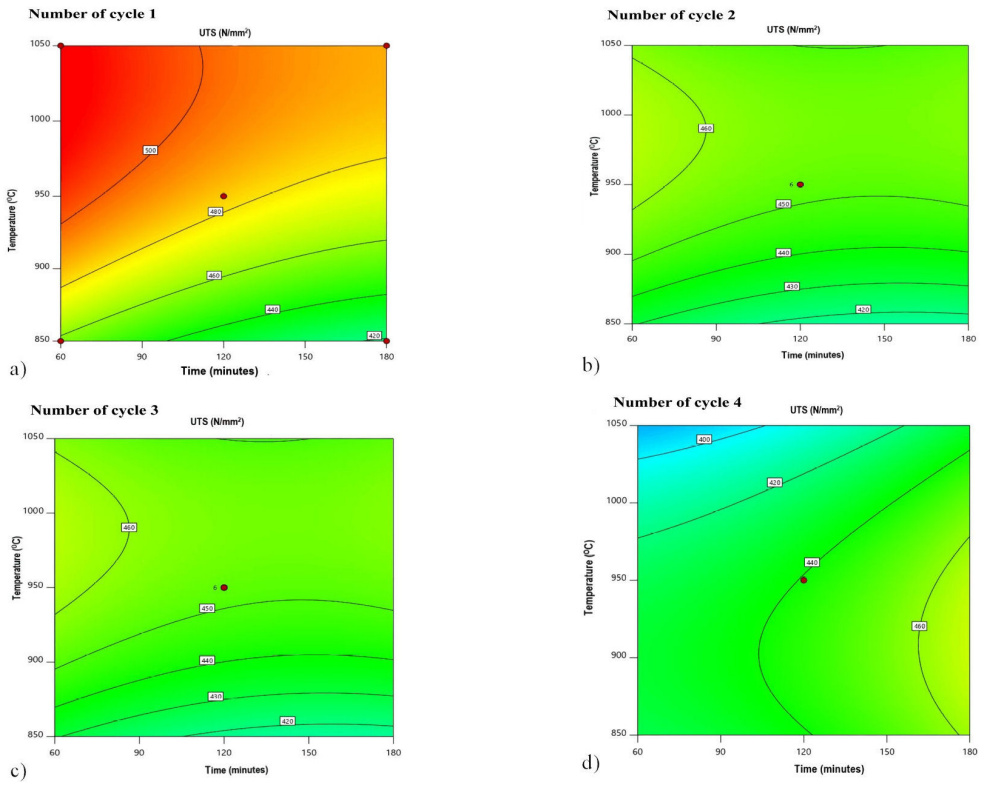

FIGURE 4. Response surface plots showing the combined effect of temperature and time on Ultimate Tensile Strength for different numbers of cycles: a) cycle 1, b) cycle 2, c) cycle 3, and d) cycle 4.

TABLE VI. Criteria for optimization parameters.

Name	Goal	Lower Limit	Upper Limit	Lower Weight	Upper Weight	Importance
A: Time	Minimize	60	180	1	1	5
B: Temperature	Is in range	850	1050	1	1	5
C: No. of Cycle	Is in range	1	3	1	1	5
Hardness	Is in range	1250	1662	1	1	5
UTS	Maximize	363	514	1	1	5

this experiment, each with a different time and temperature. Minimum cycle counts resulted in minimum hardness values between 1295HV to 1615HV, respectively. Higher hardness has been attained in the meantime by raising the higher temperature and longer prolonged time. The hardness value for number of cycle two was much greater than for cycle number one, and the diffusivity of boron concentration is lower than other parameters in low temperature conditions. The hardness of cycle three ranged from 1335HV to 1672HV, and the variation in results for Cycle 3 is seen in Fig. 3. Cycle 4 showed a lower hardness than Number of Cycle 3, although it was still better than Numbers of Cycle 1 and 2. The highest hardness value that was displayed as 1501HV.

3.2. Numerical analysis

3.2.1. Desirability approach

Multi-objective optimization was used to solve the optimization problems of the MCIBC process. The main goal of the approach is to determine the independent variable circumstances that lead to the best possible values for the output parameter. The desirability function is a function that ranges from 0 to 1, where 0 denotes an undesirable configuration and 1 denotes the ideal design for the relevant parameter (Montgomery 2019). The Desirability approach of optimized parameter is shown in figure.

The aim and factor range of this optimization issue are presented in Table VI. Each parameter has been adjusted to be of similar relevance, but the list of goals is different. The goal of Microhardness was set as range, and the goal of UTS was set as maximum. The most appropriate solution is selected based on the desired situation, and the following solutions are listed in Table VII.

3.2.2. Validation test

The Validation test compares predicted and optimal outcomes to determine the percentage of error. Table VIII shows that the error percentage between predicted and experimental values is within acceptable limits (less than 4.5%). The result indicating that the experimental and predicted values are in good agreement. The optimal parameter derived by RSM provides greater accuracy.

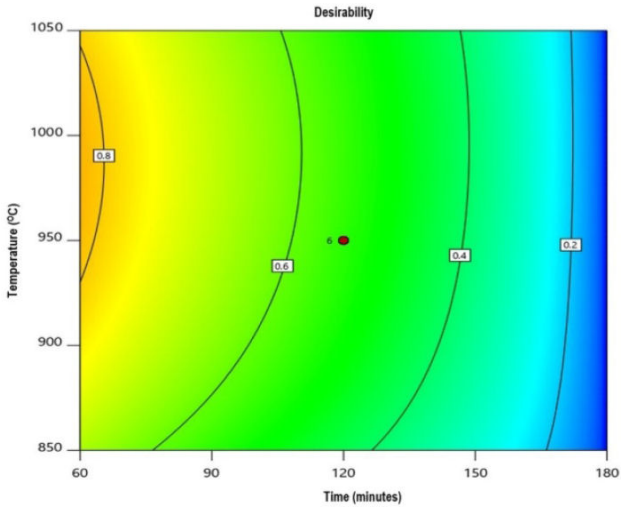

FIGURE 5. Desirability approach of optimized parameter for MCIBC process.

3.3. Microstructural modification

This work investigated the optical microstructure of multi cycle interrupted borocarburized layer formed on AISI 1020 steel with the standard method of pack boriding. The microstructures of both the processes are shown in Fig. 6. Three zones of layers are revealed *i.e.* Formation of Iron Boride (Fe_2B + FeB) layer (ii) Formation of Carburized layer with the presence of pearlite and alloyed cementite and (iii) Presence of base material at the core region of the material. In continuous boriding, three zones of layers had formed (i) poly phase iron boride zones with the formation of acicular structure, (ii) Transition zone and (iii) base material. The needles of MCIBC process exhibit shorter needles (73 μm to 126 μm) than continuous borided needles (150 μm to 205 μm). In the MCIBC Process, effect of interrupted cooling had exhibited thicker, shorter, homogenized and non-acicular borides along with the interneedle precipitates. In this project, AISI 1015 low carbon steel was employed. Continuous boriding and MCIBC processes were done using the powder pack approach. Figure 7 depicts the mechanisms of surface modification microstructure of base metal, continuous boriding, and MCIBC processes. This base metal contains 80 % of Ferrite and 20 % of Pearlite. Boron nucleates in several places on the surface at very higher temperatures.

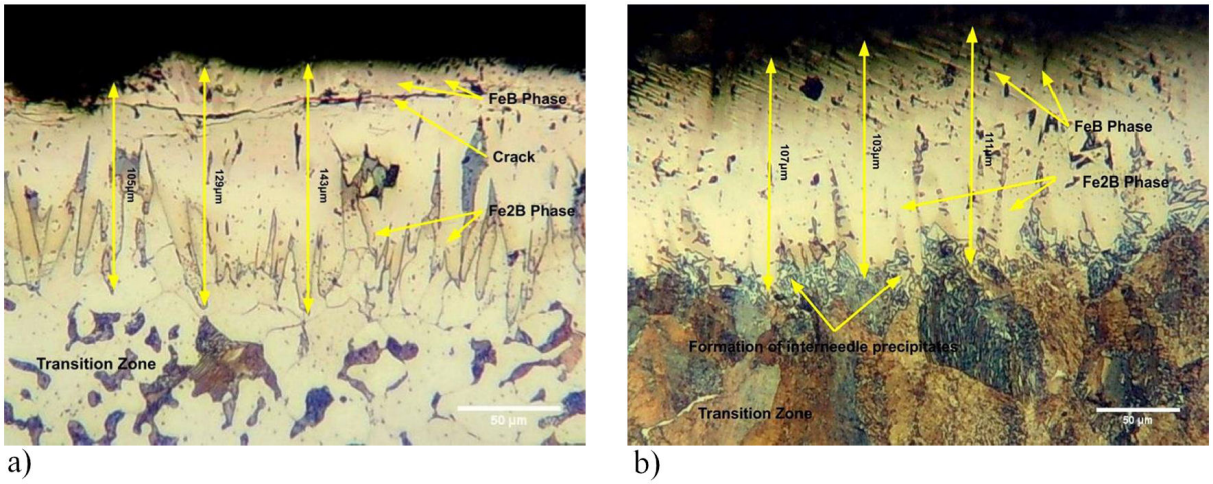

FIGURE 6. Microstructure analysis of continuous boriding and MCIBC process.

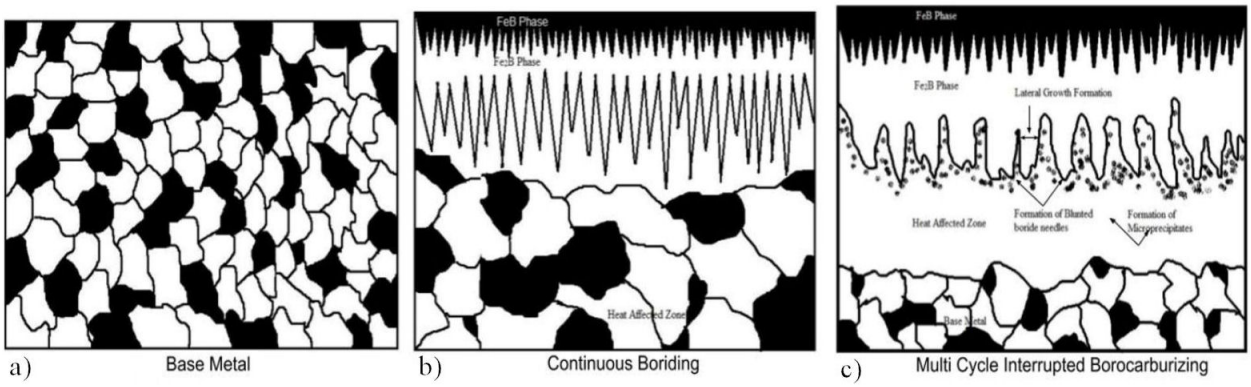

FIGURE 7. Mechanism of a) base metal, b) continuous boriding and c) multi cycle interrupted borocarburizing process.

Because of its limited solubility, boron element discards the majority of alloy elements (Litoria *et al*., 2020). The nucleation of the boron element in the continuous boriding process results in the creation of the two phase iron borides FeB and Fe_2B (Abdellah *et al*., 2014). Boride needles are structured in a non-uniform acicular pattern. It causes brittleness in the base metals surface area. A new novel technique called Multi Cycle Interrupted Borocarburizing was introduced to tackle the problem of excessive brittleness. The 950°C 60 minutes 2 Number of cycle optimal parameter was used in this procedure. In this condition, the boron atom drives the carbon atoms perpendicular to the core area (Milinovic *et al*., 2022). The cooling process causes the iron boride needles to become thicker and shorter, as well as the production of microprecipitates with Borocarbides ($Fe_3(B,C)$) or cementite (Fe_3C) (Lentz *et al*., 2018) were detected beneath the boride needles. Because of the influence of intermittent cooling, perlite to ferrite transition is greater in this zone, and grain refinement has been established below to the carburized zone.

3.3.1. Mechanisam of microstructural modification

In this project, AISI 1015 low carbon steel was employed. Continuous boriding and MCIBC processes were done using the powder pack approach. Figure 7 depicts the mechanisms of surface modification microstructure of base metal, continuous boriding, and MCIBC processes. This base metal contains 80 % of Ferrite and 20 % of Pearlite. Boron nucleates in several places on the surface at very higher temperatures. Because of its limited solubility, boron element discards the majority of alloy elements [32]. The nucleation of the boron element in the continuous boriding process results in the creation of the two phase iron borides FeB and Fe_2B [33]. Boride needles are structured in a non-uniform acicular pattern. It causes brittleness in the base metals surface area. A new novel technique called Multi Cycle Interrupted Borocarburizing was introduced to tackle the problem of excessive brittleness. The 950°C 60 minutes 2 Number of cycle optimal parameter was used in this procedure. In this condition, the boron atom drives the carbon atoms perpendicular to the core area [34]. The cooling process causes the iron boride

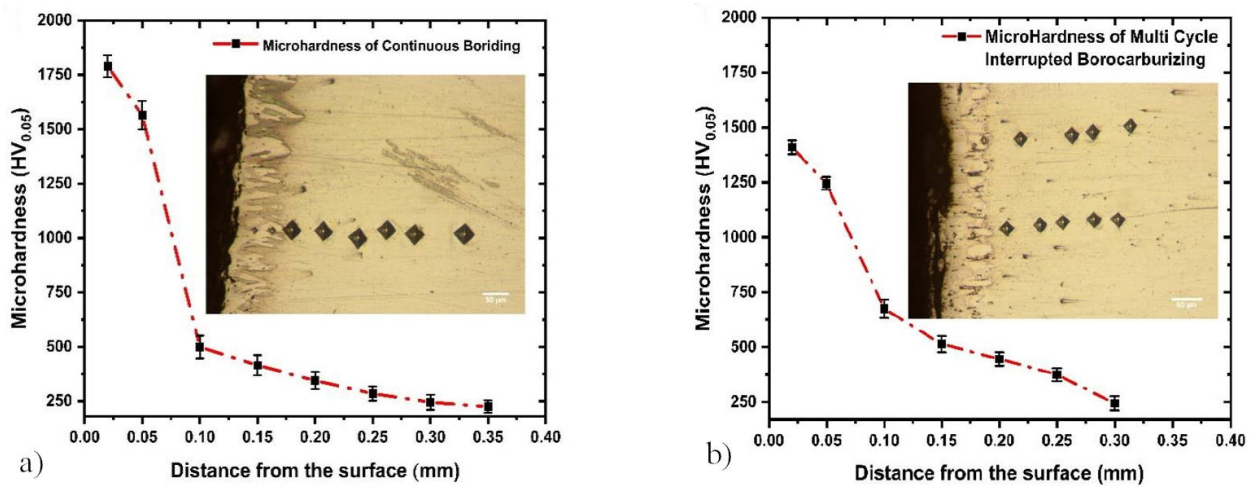

FIGURE 8. Microhardness analysis of Continuous boriding and MCIBC process.

needles to become thicker and shorter, as well as the production of microprecipitates with Borocarbides ($Fe_3(B,C)$) or cementite (Fe_3C) [35] were detected beneath the boride needles. Because of the influence of intermittent cooling, perlite to ferrite transition is greater in this zone, and grain refinement has been established below to the carburized zone.

3.4. Hardness analysis

The hardness profiles of MCIBC Process and continuous boriding process are shown in Fig. 8. At the surface region, the maximum hardness had achieved in continuous boride samples than MCIBC sample. This difference is due to the inhomogeneity of boron and carbon concentration in the surface zone of the material. In MCIBC process, the hardness gradient had gradually decreased due to the presence of carbon segregation in the transition zone. The hardness value gradually varies from $1560\,HV_{0.5}$ to $1100\,HV_{0.5}$ from surface to transition zone, then the hardness value reduced to $650\,HV_{0.5}$ in the carburized zone and $210\,HV_{0.5}$ to the base region of the metal. In continuous boriding, the presence of two phase microstructure leads to higher hardness at the surface, but the hardness gradient drops from surface to transition region. The hardness value drops from $1750\,HV_{0.5}$ to $850\,HV_{0.5}$ in the HAZ, then to $210\,HV_{0.5}$ to the base region of the material.

3.5. Phase analysis

The phase analysis had been carried for continuous boriding, and multi cycle interrupted borocarburizing processes. The presence of different forms of boride layers of various s processes was identified through X-ray diffraction (30 mA with 45 kV) using CuKα with $\lambda = 1.54060$ Å radiation. In the continuous boriding, the two phase iron borides (Fe_2B and FeB) had formed in the diffused region. In MCIBC process, the Fe_3C, Fe_2B and FeB phase had formed in the surface region of the material. The XRD graph of MCIBC is shown in Fig. 9.

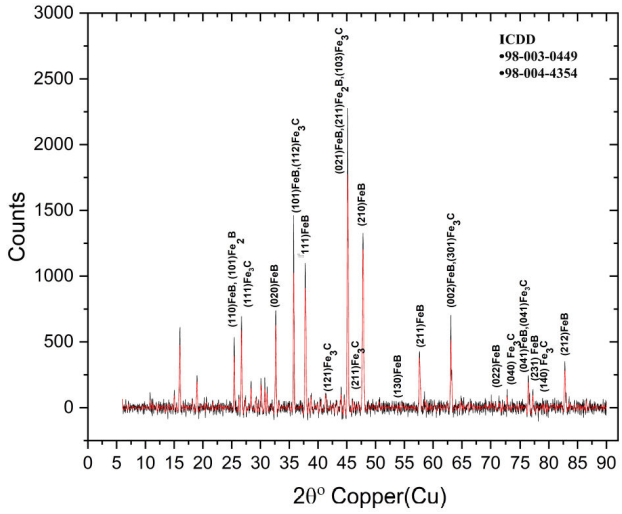

FIGURE 9. XRD pattern of the sample showing phase peaks.

3.6. Tensile analysis

The Tensile test is used to measure the parameters such as Ultimate Tensile strength, and % of elongation of Continuous boriding and MCIBC samples. The corresponding values are mentioned in Table 9. The maximum values of Ultimate tensile strength and % of elongation had attained for MCIBC as 488.276MPa, and 27.1N/mm^2. However, the yield strength value of MCIBC process exhibited lower value due to high hardness at the surface of the material and scattering of hardness at different regions. The effect of interrupted cooling with the formation of precipitates and the presence of Carburized zone had played a significant role in improving the value of UTS and strength of the MCIBC specimens.

The continuous boriding procedure caused brittle fracture of test specimens due to high hardness at the materials surface zone. At low load conditions, minimal plasticity causes fast propagation of microcracks in the ductile matrix. Figure 10 shows the mechanism of continual boriding failure behaviour.

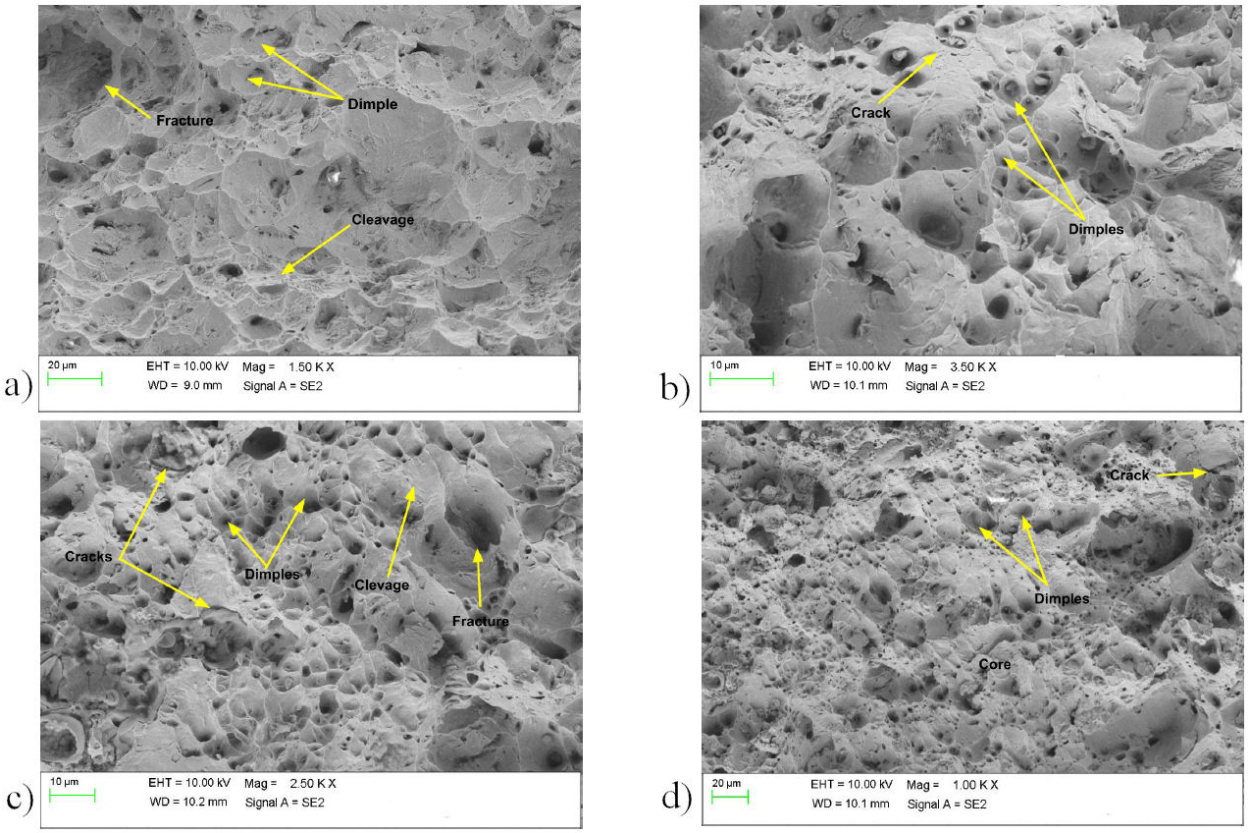

FIGURE 10. SEM analysis of fractured surface behavior of continuous boriding a), c) and mcibc process b), d) of tensile specimen

It is mentioned in the MCIBC process that following the fracture occurred in the form of brittle to ductile mode. It is worthnoting that the deformation has taken the shape of a shear mode. When compared to continuous boriding, the boride layers plasticity has improved, which tends to improve strength and reduce brittleness. The homogenous boride layer and the effect of interrupted behavior are responsible for this improvement. MCIBC mechanism was depicted in Fig. 11.

3.6.1. Fractrographic Analysis of Tensile test

The SEM Fractograph of tensile test of Continuous borided AISI 1015 Steel at 950°C 3 hours is shown in Fig. 12. Large dimples with the formation of rides were observed in the fractured zone during this process. This formation is caused by the materials continuous heating. Numerous micro cracks formed as a result of the high hardness in the surface zone.

The SEM Fractograph of the Multi Cycle Interrupted Tensile Test of AISI 1015 Steel at 950°C 2 Number of Cycle 1 Hour process time is depicted in Fig. 9. In the macro examination, the interrupted borocarburized layer exhibited brittle behavior with the development of cleavage structure. A small microprecipitation with small microcracks is observed in the transient zone as a result of the influence of interrupted cooling. The material is undamaged and the fracture acts ductile in the portion of the core.

4. Conclusion

The goal of the project is to increase the strength of the borided layer or borided steel but without much compromising the value of hardness by employing a novel technique known as Multi Cycle Interrupted Borocarburizing (MCIBC). The major influential process parameters during the process are strength and microhardness; the appropriate approach to address these multi-objective problems is response surface methodology. The empirical models for microhardness and ultimate tensile strength have been developed using the RSM technique. The optimal condition results in anticipated microhardness, and UTS of $1362\,\mathrm{HV}_{0.5}$, and 473.2 N/mm^2, respectively. It is established that the error between predicted and experimental findings is 3.48% for microhardness and 2.97% for UTS. The microstructure of the MCIBC borided sample has three different zones in the carburized zone. At the base material, the hardness reduces to $210 - 210\,\mathrm{HV}_{0.5}$. The gradient in hardness has steadily reduced from the surface of the boride layer to the base metal. The hardness of the boride layer was $1700\,\mathrm{HV}_{0.5}$ at the surface then it suddenly drops to $475\,\mathrm{HV}_{0.5}$ in the transient it represents the hardness gradient of Continuous Boriding abruptly declines from the surface of the boride layer to the base metal. The result of XRD confirms the presence of Fe_3C, Fe_2B and FeB phases in the process of MCIBC. In

the continuous boriding, Fe_2B and FeB phases are formed in the processed steel. The ultimate tensile strength of the MCIBC method was 1.23 times higher than that of the continuous boriding process. This enhancement is attributable to the behavior of the interrupted cooling and heating cycle, processed time, and temperature.

1. S. A. Kusmanov, I. V. Tambovskiy, V. S. Sevostyanova, S. V. Savushkina, and P. N. Belkin, *Surf. Coat. Technol.* **291** (2016) 334. https://doi.org/10.1016/j.surfcoat.2016.02.062
2. R. Nora, T. M. Zine, K. Abdelkader, Y. Kadi, O. Ali, and X. Jiang, *Matéria (Rio J.)* **24** (2019) e12327. https://doi.org/10.1590/S1517-707620190001.0609
3. A. K. Rai, N. Vijayashanthi, H. Tripathy, R. N. Hajra, S. Raju, S. Murugesan, and S. Saroja, *J. Nucl. Mater*. **495** (2017) 58. https://doi.org/10.1016/j.jnucmat.2017.08.011
4. M. Prince, G. S. Raj, D. Y. Kumar, and P. Gopalakrishnan, *High Temp. Mater. Process.* **26** (2022) 1. https://doi.org/10.1615/HighTempMatProc.2022041805
5. P. Jurči and M. Hudáková, *Mater. Perform. Charact.* **9** (2020) 339. https://doi.org/10.1520/MPC20190086
6. E. Hernandez-Sánchez, Y. M. Domínguez-Galicia, C. Orozco-álvarez, R. Carrera-Espinoza, H. Herrera-Hernández, and J. C. Velázquez, *Adv. Mater. Sci. Eng.* **2014** (2014) 249174. https://doi.org/10.1155/2014/249174
7. R. A. García-León, J. Martínez-Trinidad, R. Zepeda-Bautista, I. Campos-Silva, A. Guevara-Morales, J. Martínez-Londoño, and J. Barbosa-Saldaña, *Tribol. Int.* **157** (2021) 106885. https://doi.org/10.1016/j.triboint.2021.106885
8. K. Rayane, O. Allaoui, and A. Allaoui, *Acta Phys. Pol. A* **132** (2017) 521. https://doi.org/10.12693/APhysPolA.132.521
9. M. Prince and A. J. Thanu, *High Temp. Mater. Process.* **23** (2019) 1. https://doi.org/10.1615/HighTempMatProc.2019030266
10. K. M. Winter, J. Kalucki, and D. Koshel, in *Thermochemical Surface Engineering of Steels*, *Woodhead Publishing* (2015) p. 141. https://doi.org/10.1533/9780857096524.1.141
11. D. A. Santana *et al*., *Surf. Coat. Technol*. **386** (2020) 125466. https://doi.org/10.1016/j.surfcoat.2020.125466
12. I. Campos-Silva, M. Flores-Jiménez, D. Bravo-Bárcenas, H. Balmori-Ramírez, J. Andraca-Adame, J. Martínez-Trinidad, and J. A. Meda-Campaña, *Surf. Coat. Technol*. **309** (2017) 155. https://doi.org/10.1016/j.surfcoat.2016.11.054
13. M. Prince, S. L. Arjun, G. S. Raj, and P. Gopalakrishnan, *Mater. Today Proc.* **5** (2018) 25276. https://doi.org/10.1016/j.matpr.2018.10.330
14. M. Kulka, N. Makuch, P. Dziarski, D. Mikołajczak, and D. Przestacki, *Opt. Lasers Eng.* **67** (2015) 163. https://doi.org/10.1016/j.optlaseng.2014.11.015
15. P. Gopalakrishnan, S. S. Ramakrishnan, P. Shankar, and M. Palaniappa, *Metall. Mater. Trans. A* **33** (2002) 1475. https://doi.org/10.1007/s11661-002-0070-0
16. A. Calik, N. Ucar, A. Kocaslan, and S. Karakas, *Surf. Rev. Lett*. **25** (2018) 1950022. https://doi.org/10.1142/S0218625X19500227
17. I. G. Sizov, U. L. Mishigdorzhiyn, and I. P. Polyansky, in *Encyclopedia of Iron, Steel and Their Alloys* (2016) p. 346. https://doi.org/10.1081/E-EISA-120049887
18. A. Günen, E. Kanca, M. Demir, Y. Er, G. Sağlam, and M. S. Gök, *Tribol. Trans.* **60** (2017) 267. https://doi.org/10.1080/10402004.2016.1159359
19. L. G. Vanegas, M. C. Espinosa, N. L. Perrusquia, M. A. Ruiz, V. H. Domínguez, L. H. Ramírez, and L. Melo-Máximo, *Microsc. Microanal.* **27** (2021) 3406. https://doi.org/10.1017/S1431927621011703
20. M. Mathew and P. K. Rajendrakumar, *Mater. Manuf. Process.* **29** (2014) 1073. https://doi.org/10.1080/10426914.2014.901538
21. M. Kheyrodin, A. Habibolahzadeh, and S. Y. B. Mousavi, *Prot. Met. Phys. Chem. Surf.* **53** (2017) 105. https://doi.org/10.1134/S2070205117010117
22. A. Erdogan, J. Tribol. **141** (2019) 121702. https://doi.org/10.1115/1.4044859
23. A. P. Krelling, C. E. Da Costa, J. C. G. Milan, and E. A. S. Almeida, Tribol. Int. **111** (2017) 234. https://doi.org/10.1016/j.triboint.2017.03.017
24. A. I. Khuri, *Biometrics Biostat. Int. J.* **5** (2017) 87. https://doi.org/10.15406/bbij.2017.05.00133
25. D. C. Montgomery, *Design and Analysis of Experiments*, John Wiley & Sons (2017).
26. T. Turkoglu and I. Ay, *Int. J. Optim. Control Theor. Appl.* **9** (2019) 39. https://doi.org/10.11121/ijocta.01.2019.00660
27. P. D. Babu, G. Buvanashekaran, and K. R. Balasubramanian, *Tribol. Trans.* **58** (2015) 602. https://doi.org/10.1080/10402004.2014.998356
28. S. C. Atul, *Int. J. Chemtech Res*. **9** (2016) 82.
29. J. L. Arguelles-Ojeda, A. Márquez-Herrera, A. L. Saldaña-Robles, A. Saldana-Robles, M. A. Corona-Rivera, and J. Moreno-Palmerin, *Rev. Mex. Fís.* **63** (2017) 76.
30. S. Sashank, P. D. Babu, and P. Marimuthu, *Surf. Coat. Technol*. **363** (2019) 255. https://doi.org/10.1016/j.surfcoat.2019.02.036
31. M. A. Alam, H. Y. Hamdan, M. Azeem, P. B. Hussain, M. S. bin Salit, R. Khan, S. Arif, and A. H. Ansari, *J. Mater. Res. Technol*. **9** (2020) 14036. https://doi.org/10.1016/j.jmrt.2020.09.087

32. A. K. Litoria, C. A. Figueroa, L. T. Bim, C. I. Pruncu, A. A. Joshi, and S. S. Hosmani, *Philos. Mag.* **100** (2020) 353. https://doi.org/10.1080/14786435.2019.1680890

33. Z. N. Abdellah and M. Keddam, *Mater. Technol.* **48** (2014) 237.

34. A. Milinović, V. Marušić, P. Konjatić, and N. Berić, *Materials* **15** (2022) 1858. https://doi.org/10.3390/ma15051858

35. J. Lentz, A. Röttger, F. Großwendt, and W. Theisen, *Mater. Des.* **156** (2018) 113